

This manuscript has been submitted to  
the International Geoscience and Remote Sensing Symposium '86  
Zurich, Switzerland, 8-11, September 1986  
and the contents are subject to change.

This copy is to provide information prior to publication.

**VERIFICATION RESULTS FOR A TWO-SCALE  
MODEL OF MICROWAVE BACKSCATTER  
FROM THE SEA SURFACE**

by

<sup>1</sup>Willard J. Pierson, Jr. and <sup>2</sup>Mark A. Donelan

<sup>1</sup>The City College of New York  
New York, NY, USA

<sup>2</sup>Shore Processes Section  
Hydraulics Division  
National Water Research Institute  
Canada Centre for Inland Waters  
Burlington, Ontario, Canada

June 1986

## MANAGEMENT PERSPECTIVE

This paper and the companion paper (A Two-Scale Bragg Scattering Model for Microwave Backscatter from Wind Generated Waves, Donelan and Pierson), present a new model for measuring winds over the ocean using satellite borne radar and present a preliminary verification of the model. These works represent an important advance in our ability to measure wind speed and direction in a synoptic sense over the world's oceans. This in turn is a necessary step in improving weather forecasting. The model will likely be used in future weather satellites.

T. Milne Dick  
Chief  
Hydraulics Division

## PERSPECTIVE DE GESTION

La présente communication et celle qui l'accompagne (A Two-Scale Bragg Scattering Model for Microwave Backscatter from Wind Generated Waves, Donelan et Pierson) décrivent un nouveau modèle de mesure des vents au-dessus des océans à l'aide d'un radar spatial et font état d'une vérification préliminaire du modèle. Ces travaux font progresser de façon importante notre capacité de mesurer à l'échelle synoptique la vitesse et la direction des vents au-dessus des océans du monde, ce qui est indispensable pour améliorer la prévision météorologique. Le modèle sera vraisemblablement utilisé dans de futurs satellites météorologiques.

Le chef,  
T. Milne Dick  
Division de l'hydraulique

## RÉSUMÉ

Le modèle de rétrodiffusion de Donelan et Pierson (réf. 6) a été ajusté à la bande  $K_u$ , sur la fréquence de 13,9 GHz. Des données des bandes L à  $K_a$  servent maintenant à tester le modèle. En règle générale, il n'existe pas de loi de puissance. Quand la vitesse du vent tombe en deçà de certains seuils, il peut ne pas y avoir de rétrodiffusion de Bragg détectable. Enfin, il peut se produire une saturation à vents de vitesse élevée. Des résultats du SEASAT-SASS servent à étoffer les prévisions du modèle et on propose certaines expériences critiques qui permettront de vérifier la validité globale du modèle.

Mots clés: rétrodiffusion, vents, lois de puissance,  
température de l'eau

# VERIFICATION RESULTS FOR A TWO-SCALE MODEL OF MICROWAVE BACKSCATTER FROM THE SEA SURFACE

Willard J. Pierson Jr.

The City College of New York, N.Y.  
U.S.A.

Mark A. Donelan

National Water Research Institute  
Burlington, Ontario, Canada.

## ABSTRACT

The backscatter model of Donelan and Pierson (Ref. 6) was adjusted to fit Ku-Band at 13.9 GHz. Data from L to Ka-Band are being used to test the model. In general, there is no power law. When the wind drops below certain threshold speeds there may be no detectable Bragg backscatter. Moreover, saturation may occur at high winds. Results from the SEASAT-SASS are used to substantiate the predictions of the model, and suggestions are made for experiments that will be critical for determining the overall validity of the model.

Key Words: Backscatter, winds, power laws, water temperature.

## 1. INTRODUCTION

The radar scattering model summarized by Ref. 6 is described in Ref. 5. For high incidence angles and high winds, the effects of spilling breakers and wedges (Refs. 1, 7, 8, 14) need to be incorporated and would increase the backscatter compared to a Bragg model, especially for horizontal polarization.

Studies of radar scattering from L to Ka-Band and wind data are under way. In a general sense, the model given in Ref. 5 agrees with these data. Data from the SEASAT-SASS program can be used to support some of the theoretical results.

## 2. THRESHOLD WINDS AND WATER TEMPERATURES

The square bracket in the equation for the high wavenumber capillary-gravity part of the spectrum (Ref. 6) at upwind can be set to zero and solved for the wind at  $\lambda/2$ , or  $\pi/k$ . The result is Eqn. (1) where  $C(k)$  is the phase speed of the waves,  $\nu$  is the viscosity of water, which increases by about a factor of two as the temperature varies from 30°C to 0°C, and  $D$  is  $0.194 \rho_a/\rho_w$ .

$$\bar{U}(\pi/k) > C(k) + 2(\nu k C(k)/D)^{1/2} \quad (1)$$

A drag coefficient for a boundary layer wind represented by  $CDN$  for a neutrally stratified atmosphere is also needed as on Fig. 1. This permits the computation of the wind at  $\bar{U}(\pi/k)$ , given the wind at 10 m. The RHS of (1) is a function of wavenumber and water viscosity. According to the model, the LHS must be greater than the RHS for

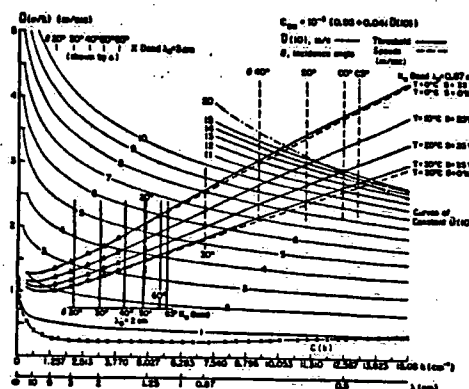


Fig. 1. Threshold wind speeds for significant Bragg backscatter for three bands. Abscissa;  $k$  in  $\text{cm}^{-1}$ , or  $\text{cm}$ . Ordinate, wind speed at  $\pi/k$ , or  $\lambda/2$ . Lines of constant wind speed at 10 m as a parameter. Threshold speeds, for four temperatures for salinities of 0‰ and 35‰. Incidence angles from 20° to 65°. Phase speed,  $C(k)$ . Unless the curve for constant  $\bar{U}(10)$  lies above the threshold speed, Bragg backscatter will probably be too low to detect.

there to be any waves with the wavenumber used in the equation to exist in the spectrum.

Fig. 1 shows the result of applying Eqn. (1) to three bands. The upward sloping lines show the combined effect of  $\nu$ ,  $k$  and  $C(k)$ . Given a water temperature and salinity, unless the wind at  $\pi/k$  lies above the corresponding line there will be no spectral components present in the wavenumber spectrum as illustrated in Ref. 6. The vertical lines and triangles show the wavenumbers appropriate to various incidence angles for three bands as described by the wavenumber,  $2k_0 \sin \theta$ .

For an incidence angle of 60° and sea water with a temperature of 0°C, a wind of 6 m/s for Ku-Band is needed to generate a spectral Bragg component in equilibrium with the wind. In contrast, at a 30° incidence angle for water at 30°C a wind of only about 2.7 m/s is needed.

It has been estimated that about 20% of the areas

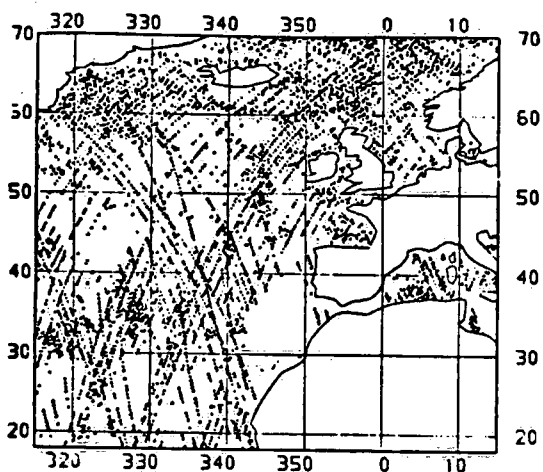


Fig. 2. Discarded SASS data for six days during the lifetime of SEASAT for western North Atlantic. For the triangles, the value of  $K_p$  was greater than one. For the plus signs, the estimates of received power were negative.

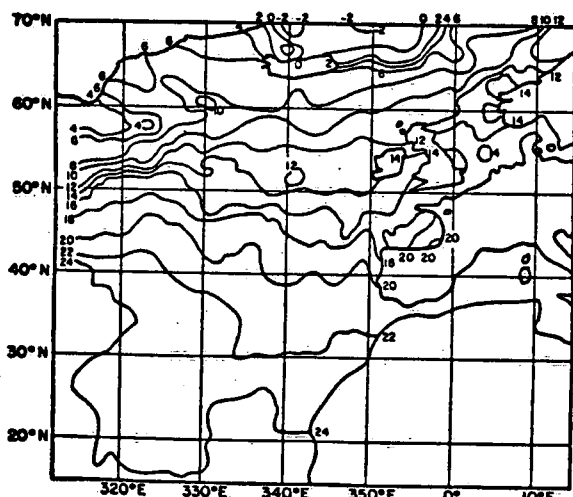


Fig. 4. Sea surface isotherm fields near the time of Fig. 2.

sampled by the SEASAT-SASS returned values of the telemetered data that upon further processing were not used to recover information about the winds. (Personnel communication, D. Boggs and P. Woiceshyn). The scatterometer on SEASAT measured the power in the signal (the desired received backscatter power) plus the power of the noise  $P_{SN}$ , in the system as  $P_S + N_1$  where the circumflex indicates that the quantity is a random variable. The instrument then measured the noise alone separately as  $N_2$ . Both of these quantities are normally distributed random variables. They have large enough average values and small enough variances so that a negative value is highly improbable for either measurement. The received power,  $P_R$ , to be used in the radar equation was then computed from the difference,  $P_{SN} - N_2$ .

If the average power of  $N_1$  equals the average

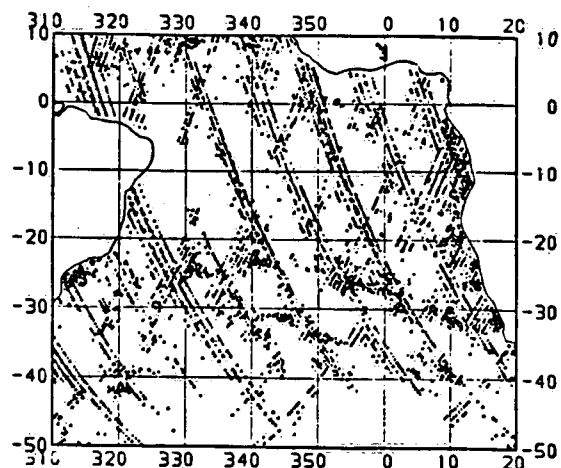


Fig. 3. Discarded SASS data for six days during the lifetime of SEASAT for portions of the Equatorial and South Atlantic. Coded as in Fig. 2.

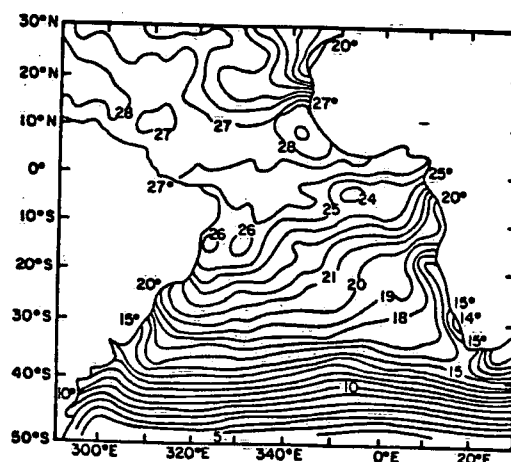


Fig. 5. Sea surface isotherm fields near the time of Fig. 3.

power of  $N_2$  (in an oversimplified sense since corrections of various kinds are needed, see Ref. 3)  $P_R$  then provides an estimate in a statistical sense of the received backscatter power to be used in the radar equation. The difference between two large measurable non-zero random numbers with expected values that differ by small amounts can be negative. The randomly varying estimate of the backscatter,  $\hat{\sigma}^0$  has a normal distribution with an expected value,  $\sigma^0$  and a variance given by  $A(\sigma^0 + B)^2 + C$  where  $\sigma^0$  is the "true" value from a correct model function. A, B and C are known constants. If  $\sigma^0$  is zero, a probability for a random value of  $\hat{\sigma}^0$  still exists.

If the backscattered power,  $\hat{P}_R$ , is very small, or perhaps non-existent, the result could be either positive or negative with equal probability. Thus if the expected (in a statistical sense) value of  $\sigma^0$  is zero, the estimated, or "measured", value of  $\hat{\sigma}^0$  will be equally likely to be positive or negative. Negative estimates of  $P_R$  were discarded.

A quantity  $K_p$  was also used incorrectly. Effec-

tively, what was computed can be shown to be equivalent, more or less, to evaluating  $(A(\sigma^0 + B)^2 + C)^{1/2}/\sigma^0$ . As  $\sigma^0$  approaches zero,  $K_p$  approaches infinity. Those values of the backscatter that gave a value of  $K_p$  greater than one were also discarded.

For the first six days of the operation of SEASAT-SASS, D. Boggs has prepared world plots for both vertical and horizontal polarization that show how often negative values of  $P_R$  were obtained by the SASS and how often the data were not used because  $K_p$  was greater than one. The full charts are most instructive and illustrate features of the climatology of the winds for July 1978 and the distribution of sea surface temperatures.

Two charts also prepared by Boggs are shown in Figs. 2 and 3 for vertical polarization data. During this time, the orbit of SEASAT shifted slowly westward from one day to the next. For example, the five rows of points in Fig. 3 starting near 340°E and 40°S and ending at the Coast of South America between 10°S and 20°S represent five successive days of northbound passes over the South Atlantic Ocean, probably for points at the outer edge of the swath. Triangular clusters of points represent the combined effect of northbound and southbound passes about 12 hours apart as illustrated in Fig. 3 near 340°E and 20°S.

A row of points can be followed on one of these figures. For some areas the points are nearly all small triangles, and this pattern indicates detected values of the received power, which though small, could represent the effect of light winds. Other rows show a random sequence of triangles and plus signs, and this pattern indicates very weak or non-existent backscattered power such that both positive and negative values for the estimates were equally probable.

Near the dominant tracks for each figure, additional points can often be found. They are particularly dense off the west coast of Africa from 30°S to the Equator, to the south of Greenland and in the area between 30°N and 40°N west of the Straits of Gibraltar.

Figs. 4 and 5 show the sea surface temperature fields based on a GOSSTCOMP analyses (supplied by the Marine Products Branch of NMC of NWS of NOAA) for a date close to the time that the SASS data were obtained. In Fig. 4, the sea surface temperature field varies from -2°C near Greenland north of Iceland to 24°C in the southernmost areas. In Fig. 5 the strong temperature gradient from 40° to 50°S is noteworthy along with a 4°C temperature gradient off the west coast of Africa as a combined result of the Benguela current and upwelling. This pattern persisted throughout the entire month of July, 1978. Presently available temperature fields are far superior to these with greater accuracy as described by Strong and McClain (Ref. 12) and higher resolution.

The concatenation of threshold wind speeds with sea surface temperatures is marked in these figures. For Figs. 2 and 4 off Greenland over water colder than 6°C for high incidence angles, the winds would only have to be below about 5 m/s to cause the data to be discarded. Northeast of a line between England and Iceland over 2°C to 10°C water, the winds could be between 5 and 6 m/s, and the data would still have been discarded. To the west of

Gibraltar, the Bermuda-Azores subtropical high is usually quite strong in July. The greater density of points for lower incidence angles over water from 20°C to 24°C indicates winds under 3 to 3.5 m/s. The North Sea, with water of 14°C, has much fewer drop outs than farther to the northwest. Northbound orbits that cross the area from 30°N to 40°N and 340°E to 350°E show that the southeast portion of this region had winds over 4.5 to 5 m/s.

A comparison of Figs. 3 and 5 shows many interesting features of the Equatorial and South Atlantic. The temperature field shows an eastwest temperature gradient of 3°C to 5°C over a relatively short distance to the west of the African coast. These colder waters, combined with the lighter winds of the subtropical high, resulted in a high density of discarded data from the southern tip of Africa to the Equator. For the 14°C isotherm and a 30° incidence angle, the wind would have had to have been under about 3.2 m/s. In the latitude band between 40° and 50° with water from 10° to 5°C the limited number of drop outs suggest that the winds usually exceeded 5.0 to 5.5 m/s. North of a line joining the Equator at 320°E and the coast of Africa at 10°N, there are a large number of discarded data for 27° to 28°C water associated with the doldrums and winds for a 30° incidence angle of less than 3.2 m/s.

Intriguing features of Fig. 5 are two bands locating data that were discarded whose northern edges can be traced from east to west by their latitude-longitude locations. The first band starts near 10°E, 28°S and then moves to 0°E, 22°S; 350°E, 21°S; 340°E, 20°S; 330°E, 20°S and perhaps, 320°E, 22°S. The second band starts at 10°E, 39°S and continues westward to 0°, 34°S; 350°E, 32°S and perhaps to 340°E, 30°S.

The isotherm fields that were then available are probably too oversmoothed to show what may really have happened. That strong temperature gradients across oceanic fronts exists in these areas was reported by Deacon with temperature changes of 8°C for the subtropical convergence and 5°C for the Antarctic convergence whose general locations were indicated by DeFant. (Ref. 9).

More recent sea surface temperature fields for the southern oceans are beginning to delineate these convergences in both the South Atlantic and the Indian Ocean with a resolution of 100 km. There is some degree of smoothing because clouds interfere with the measurement of the infrared radiation from the ocean, and continuity from past data is used to fill in the gaps. A study of the sea surface temperature fields for this area of the South Atlantic when combined with data from future scatterometers should be informative. It may be possible to detect these convergences even through clouds.

Given the sea surface temperature, the incidence angle at which the backscatter data first begin to exhibit equally probable positive and negative estimates of backscatter, as also affected by gustiness and cats-paws, is an indication of the threshold wind in Fig. 1. Light winds can be expected over relatively large areas of the ocean so that the potential exists for resolving wind speeds across the swath from about 2 to 4 m/s in tropical areas and from about 3 to 5 m/s in polar areas.

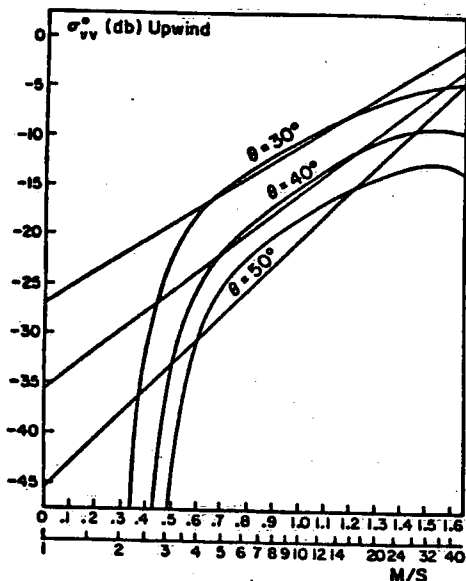


Fig. 6. Example power law models for 30°, 40° and 50° at upwind compared to the model (Ref. 6) for 30°C water.

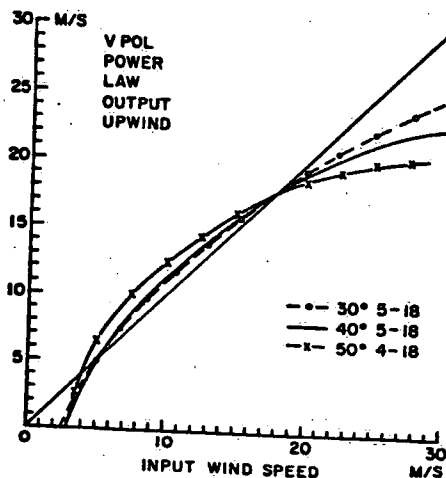


Fig. 7. Output winds for an assumed vertically polarized power law model for three incidence angles if the true model is (Ref. 6) as a function of input wind speed.

### 3. COMPARISONS WITH POWER LAW MODELS

A power law model assumes that radar backscatter in decibels,  $\sigma_{db}^0$  can be described by  $G(X, \theta) + H(X, \theta) \log_{10} U$  as a function of incidence angle, aspect angle and the effective neutral wind at 19.5 m.

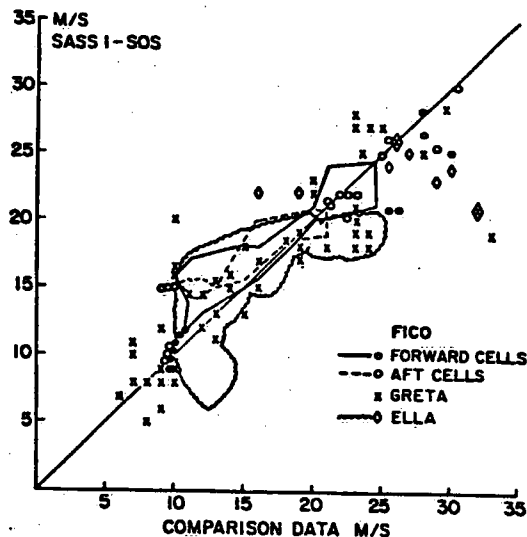


Fig. 8. Composite of winds speeds recovered by the SASS-1-SOS wind recovery algorithm compared to winds from Hurricanes Fico, Greta and Ella.

There are numerous power law fits in the literature for C, X, Ku and Ka-Band, with a large number of them especially for Ku-Band. The most common feature of these power law fits is that they disagree with each other by very large amounts, even at times for identical data bases. Other common features are that the backscatter measurements for low winds may have been contaminated by noise in the receiver channels used for the radar, data for light winds for which measurements were attempted but not made have not been reported, the data have not been stratified according to water temperature, and the power law model has been extrapolated to high wind speeds for which no backscatter measurements were made. The power law model described by Ref. 11 has these and other sources of error when combined with the SOS wind recovery algorithm as documented, by Ref. 15.

It is manifestly impossible to fit a straight line to a family of water temperature dependent curved lines as in the figure in Ref. 6. To illustrate the errors inherent in wind recovery algorithms that use a power law, power laws have been assumed for incidence angles of 30°, 40° and 50° and graphed in Fig. 6 as a simplified version for a water temperature of 30°C. For 30° and 40° incidence angles the power laws have been chosen to agree with our model at wind speeds of 5 and 18 m/s. For 50°, the wind speeds are 4 and 18 m/s.

For winds speeds less than 5 m/s at a 30° and a 40° incidence angle, our model predicts that the expected value of the backscatter will be less than the value required by the power law, with the same being true at a 50° incidence angle for 4 m/s. Between 5 (or 4) and 18 m/s, our model predicts higher backscatter values than the power law, and above 18 m/s, it predicts lower values.

Suppose that our model correctly predicts the backscatter, that the assumed power law for a 50° incidence angle had been used and that a measurement

of backscatter looking upwind had been made for a wind of 6 m/s. The power law would then give a wind of 8 m/s.

The wind speeds that would be recovered by the assumed power laws, given that our model is correct, have been scaled from Fig. 6 and graphed in Fig. 7 for input winds up to about 29 m/s, or nearly hurricane speeds. For the assumed power laws, an input wind of 29 m/s yields a wind from the power law between 20 and 25 m/s for vertical polarization. The winds recovered from a power law model would be too low for light winds and high winds and too high for winds of intermediate speeds.

Fig. 8 is a composite of scatter plots from Black, et al. (Ref. 2), who compared winds recovered by the SASS-1-SOS wind recovery algorithm with winds obtained in various ways from ship reports, aircraft flights, low level cloud motions and numerical models for Hurricanes Fico, Greta and Ella. Where the points are too numerous to plot, the point cloud has been outlined by coded lines. There are additional sources of error in the SOS wind recovery algorithm for light winds even if the power law assumption were correct. Also the scatter is enhanced by whatever errors there are in the wind speeds from the comparison data.

Nevertheless, Fig. 8 shows that the general features of Fig. 7 are verified by comparisons of winds obtained some other way and winds recovered by the SASS-1-SOS model function and wind recovery algorithm. Ref. 2 attribute the bias for high winds to the effects of the attenuation of the radar measurements by clouds and rain. The bias for intermediate winds cannot be explained in this way. Delnore, et al. (Ref. 6) report similar results for aircraft measurements of backscatter during a hurricane. Passive microwave measurements were used in Ref. 6 to eliminate the possibility of attenuation, and the decreased sensitivity of backscatter to increasing wind speed was still present.

In the analysis by Woiceshyn, et al. (Ref. 15), there were no winds over 25 m/s recovered for V-pol whereas winds over 33 m/s were recovered for H-pol. Their Figs. 10a, b and c all support the predictions of our model for V-pol for winds above 8 m/s. The rejection of low backscatter values by the SOS algorithm and the effects of temperature mask the predicted effects of our model for light winds in these results. See Ref. 10.

This paper and Ref. 6 do not illustrate the additional effects of backscatter from the wedge-like crests of waves about to break and from spilling breakers. These effects would produce backscatter values for vertical polarization that could be somewhat higher than the values in Fig. 6 which treats Bragg scattering waves tilted by the longer gravity waves. Horizontally polarized backscatter is about 10 db lower than vertically polarized backscatter for high incidence angles and high winds and for a Bragg theory. Ref. 5 shows that these additional effects are very important for horizontal polarization and cannot be neglected.

#### 4 SUGGESTED EXPERIMENTS

To verify further the results of our model for backscatter from waves when the winds are light, experiments need to be made over very warm water and very cold water. The winds would need to be measured by a suitably responsive anemometer, and

the aircraft with the radar would need to fly at a low altitude. The receiver noise in the radar would need to be measured accurately. Appropriate probabilistic and statistical models would be needed to decide whether or not the received power was below the level of detection by the radar. The waves would also need to be recorded carefully so as to obtain spectral estimates because a swell or a dead sea could be present that would tilt Bragg scatterers by amounts greater than those for a fully developed sea at the low wind speeds of the experiment. Other effects should be relatively unimportant.

For high winds and high waves at high incidence angles, backscatter will also depend to some extent on the state of development of the waves. The wave and weather measuring data buoys that have been deployed by various nations could be used if longer wind averages were obtained. The aircraft system described in Ref. 14 could obtain wavenumber spectral estimates. A way to quantify the number and shapes of breakers and wedges needs to be described.

#### 5. CONCLUSIONS

Backscatter from the ocean surface depends directly on the properties of the waves on the ocean. The spectrum of the Bragg waves depends on water temperature. The properties of breakers and wedges for high wind are fetch and duration dependent as well as wind speed dependent. Data from the SEASAT-SASS support the model we have described. A wind recovery procedure that accounts for these effects should vastly improve the determination of wind speeds and directions from scatterometers by removing the biases in power law models especially for winds from 18 to 29 m/s. Horizontally polarized backscatter at the higher incidence angles will quite possibly provide data that can be used to recover even higher winds. Additional experiments are needed.

#### 6. ACKNOWLEDGEMENTS

We appreciate the help of D. Boggs. W. G. Pichel provided the GOSSTCOMP charts. The contribution of W. J. Pierson to this paper was sponsored by NASA under Grant NAGW-690.

#### 7. REFERENCES

1. Banner M L and Fooks E H 1985, On the microwave reflectivity of small-scale breaking water waves, *Proc Roy Soc Lond A* 399. 93-109.
2. Black P G, Gentry R C, Cardone V J and Hawkins J D 1985, SEASAT microwave wind and rain observations in severe tropical and mid-latitude marine storms. in Saltzman, B. ed *Satellite Oceanic Remote Sensing*, Advances in Geophysics, 27, 197-277.
3. Bracalante E M, Boggs D H, Grantham W L and Sweet J L 1980, The SASS scattering coefficient  $\sigma^0$  algorithm, *IEEE J Oceanic Eng*, oe-5(2), 145-154.
4. Delnore V E, Bahn C S, Grantham W L, Harrington R F and Jones W L 1985, Active and passive microwave measurements in Hurricane Allen, NASA Langley Res Center, NASA TN-86390. Nov.

5. Donelan M A and Pierson W J 1986, Radar-scattering and equilibrium ranges in wind-generated waves-with application to scatterometry, (Submitted to *J Geophys Res Oceans*).
6. Donelan M A and Pierson W J 1986, A two scale Bragg scattering model for microwave backscatter from wind generated waves, (*This symposium*).
7. Kwoh D S W and Lake B M 1984, A deterministic, coherent, and dual-polarized laboratory study of microwave backscattering from water waves, Part I: Short gravity waves without wind, *IEEE J Oceanic Eng. OE-9*, 5, 291-308, Dec.
8. Lyzenga D R, Maffett A L and Shuchman R A 1983, The contribution of wedge scattering to the radar cross section of the ocean surface, *IEEE Trans Geoscience Remote Sensing GE-21*, 4, 502-505, Oct.
9. Neumann G and Pierson W J 1966, *Principles of Physical Oceanography*, Prentice Hall, Englewood Cliffs, NJ. 545 p.
10. Pierson W J, Sylvester W B and Donelan M A 1986, Aspects of the determination of winds by means of scatterometry and of the utilization of vector wind data for meteorological forecasts, *J Geophys Res* 91, (2), 2263-2272.
11. Schroeder, L C, Boggs D H, Dome G, Halberstam I M, Jones W L, Pierson W J and Wentz F J 1982, The relationship between wind vector and normalized radar cross section used to derived SEASAT-A satellite scatterometer winds, *J Geophys Res*, 87, 3318-3336.
12. Strong A E McClain E P 1984, Improved ocean surface temperatures from space-comparisons with drifting buoys, *Bull Amer Meteor Soc*, 65, 2, 138-142.
13. Walsh E J, Hancock II D W, Hines D E, Swift R N and Scott J F 1985, Elimination of directional wave spectrum contamination from noise in elevation measurements, *IEEE J Ocean Eng OE-10*, 4, 376-382.
14. Wetzel L 1986, On microwave scattering by breaking waves in Hasselmann, K. and Phillips, O. M. *eds Wave Dynamics and Radio Probing of the Ocean Surface*, Plenum Press.
15. Woiceshyn P M, Wurtele M G, Boggs D H, McGoldrick L F and Peteherych S 1986, The necessity for a new parameterization of an empirical model for wind/ocean scatterometry, *J Geophys Res* 91, (C2), 2273-2288.

#### APPENDIX A

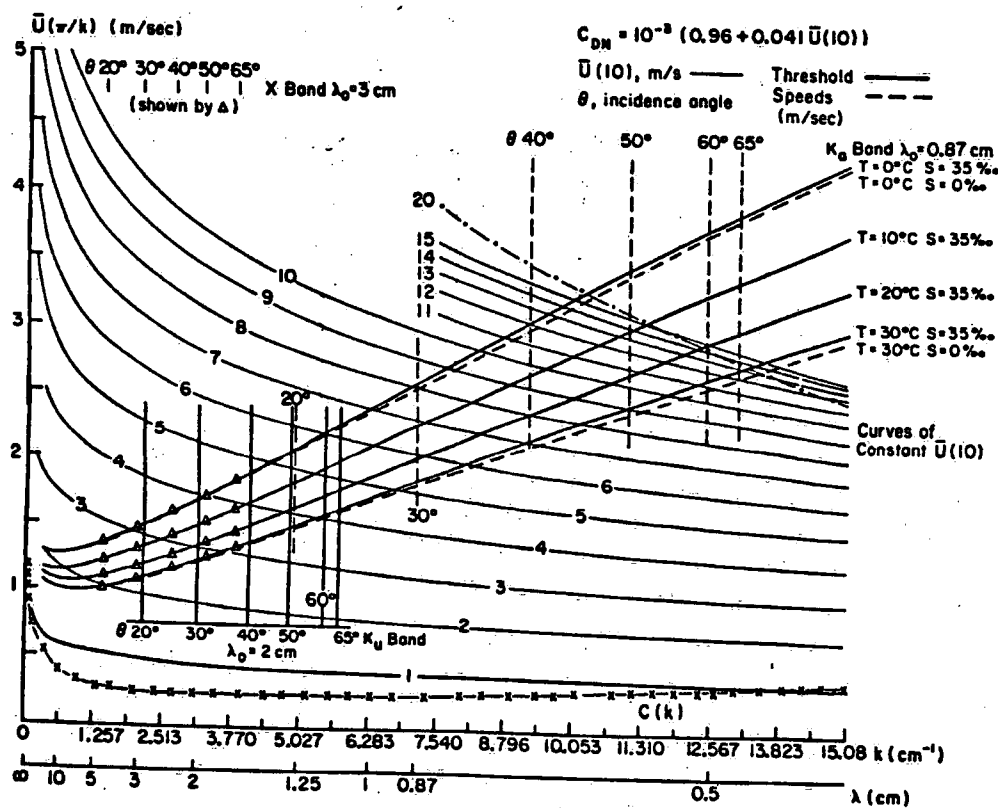


FIG. A-1 Large Version of Fig. 1.